

Minidisk Influence on Flow Variability in Accreting Spinning Black Hole Binaries: Simulations in Full General Relativity

Jane C. Bright,¹ Vasileios Paschalidis,^{1,2}

¹ Department of Astronomy, University of Arizona, Tucson, AZ 85726, USA

² Department of Physics, University of Arizona, Tucson, AZ 85726, USA

31 October 2022

ABSTRACT

We perform magnetohydrodynamic simulations of accreting, equal-mass binary black holes in full general relativity focusing on the effect of spin and minidisks on the accretion rate and Poynting luminosity variability. We report on the structure of the minidisks and periodicities in the mass of the minidisks, mass accretion rates, and Poynting luminosity. The accretion rate exhibits a quasi-periodic behavior related to the orbital frequency of the binary in all systems that we study, but the amplitude of this modulation is dependent on the existence of persistent minidisks. In particular, systems that are found to produce persistent minidisks have a much weaker modulation of the mass accretion rate, indicating that minidisks can increase the inflow time of matter onto the black holes, and dampen out the quasi-periodic behavior. This finding has potential consequences for binaries at greater separations where minidisks can be much larger and may dampen out the periodicities significantly.

Key words: black hole physics—gamma-ray burst: general—gravitation—gravitational waves—stars: neutron

1 INTRODUCTION

Supermassive black hole (SMBH) binaries are expected to form in gas rich environments as a result of galaxy mergers [Rodriguez et al. \(2009\)](#). The central SMBHs from each galaxy in the merger are driven to form a bound binary due to dynamical friction, followed by stellar and other environmental interactions which can bring them to close separations, where the subsequent evolution is driven by gravitational wave emission (see, e.g., [Mayer et al. \(2007\)](#)). SMBH binaries are particularly promising systems for multi-messenger astronomy with gravitational waves. Gravitational waves from SMBH binaries are expected to be detectable by Pulsar Timing Arrays or by future space-based gravitational wave observatories such as the Laser Interferometer Space Antenna (LISA) [Hobbs et al. \(2010\)](#); [Amaro-Seoane et al. \(2017\)](#), [Amaro-Seoane et al. \(2022\)](#), [Barausse et al. \(2020\)](#), [Arun et al. \(2022\)](#).

Theoretical models make predictions about what the environments around accreting SMBHBs could look like. When the gas around the binary has sufficient angular momentum, the two black holes are expected to be surrounded by a circumbinary accretion disk with the black holes located in a low density central “cavity” that is cleared by the binary tidal torques [Artymowicz & Lubow \(1994\)](#), [Milosavljević & Phinney \(2005\)](#), [Kocsis et al. \(2012\)](#), [MacFadyen & Milosavljević \(2008\)](#). Accretion into the central cavity then proceeds through two tidal streams, and can form minidisks around the individual black holes. Shock heating of the minidisks may make them responsible for enhancement of emission in the

hardest parts of the electromagnetic spectrum, see e.g., [Sesana et al. \(2012\)](#), [Roedig et al. \(2014\)](#), [Farris et al. \(2015b\)](#).

Binary systems within the gravitational-wave driven regime cannot be observationally resolved by existing telescopes unless they are extremely close to our Galaxy. Furthermore, it can be challenging to distinguish a binary from a regular single black hole system electromagnetically. Periodicities in quasar light curves may be able to help identify systems containing binaries and distinguish them from single black hole systems. Therefore, the key frontier in theoretical work to-date has been to identify smoking-gun electromagnetic signatures that accompany the gravitational wave signal and which can be used to guide electromagnetic observations. Several mechanisms have been proposed that may cause periodicities from binaries: Doppler boosts along our line of sight of emission from gas bound to the moving black holes [D’Orazio et al. \(2015\)](#), gravitational lensing of the accretion onto one of the black holes by the companion black hole [D’Orazio & Di Stefano \(2018\)](#), and variability in accretion rates onto the black holes in the binary (see also [Bogdanović et al. \(2022\)](#) for a recent review of electromagnetic emission from SMBH binary mergers). Periodic accretion has been associated with an over-dense “lump” feature forming on the inner edge of the circumbinary disk caused by material from the accretion streams being flung outward and breaking the axisymmetry. This lump then modulates the accretion onto the minidisks, feeding more material to the black holes in a periodic way [Noble et al. \(2012\)](#), [Shi et al. \(2012\)](#), [Farris et al. \(2014\)](#), [Gold et al. \(2014a\)](#), [Noble et al. \(2021\)](#). Recent studies suggest that the periodicities in accretion

rate are modulated by the lump relating to the beat frequency of the lump's orbital frequency and the binary's orbital frequency [Bowen et al. \(2018\)](#), [Bowen et al. \(2019\)](#), [Combi et al. \(2022\)](#).

However, variability of the mass accretion rate should depend on the matter inflow time from the minidisks. In particular, if the inflow time from the minidisks is longer than the modulation of the accretion flow due to the binary orbit, then one could expect that such periodicities can be phased out by the minidisks, in which case periodicities in the electromagnetic lightcurves could not be attributed to accretion rate modulation by the binary orbit. Interestingly many relativistic studies of accreting binaries near merger do not exhibit large and persistent minidisks, while Newtonian studies with parametrized inflow time from the minidisks have reported such minidisks. The inflow time from the minidisks is an unresolved question, and it could depend on many physical parameters including black hole spin magnitude and orientation, binary mass ratio, magnetic flux in the circumbinary disk, et cetera. Given that periodicities in quasar lightcurves are often viewed as modulations due to the binary orbit, it is important to resolve when such quasi-periodic behavior in the accretion rate onto the black holes is possible. This requires that we determine if and when the inflow time from the minidisks becomes comparable or longer than the binary orbital period especially for binaries in the gravitationally wave driven and highly dynamical spacetime regime. Another question is whether such binaries at relativistic orbital separations are relevant at all for current electromagnetic separations. In this work we begin to address these questions.

Photometric surveys have been implemented to perform systematic searches for SMBHBs identifiable through periodicities in their light curves, leading to about 200 current SMBH binary candidates [Graham et al. \(2015\)](#), [Charisi et al. \(2016\)](#). SMBHBs at relativistic orbital separations of a few tens to a hundred gravitational radii are likely observationally relevant. This is demonstrated explicitly in [Fig. 1](#), where we plot the reported orbital separation vs. mass for 50 candidate SMBHBs with 3 or more cycles of periodicity in their lightcurves as compiled in [Liu et al. \(2019\)](#). In [Liu et al. \(2019\)](#) the orbital separation is given in pc, so here we have converted the orbital separation to units of gravitational radius using the mass estimate for these systems. As is clear from the plot about 20 candidates are inferred to have orbital separation $\lesssim 40GM/c^2$ (where M is the total binary gravitational mass), and about 10 have an orbital separation $\lesssim 25GM/c^2$, where general relativity is particularly important to determine the magnetohydrodynamic flow onto the SMBH binaries. Therefore, binaries at relativistic orbital separations are observationally relevant.

Circumbinary accretion has been investigated through both Newtonian and relativistic simulations. Newtonian studies that have studied circumbinary accretion include [MacFadyen & Milosavljević \(2008\)](#), [D'Orazio et al. \(2013\)](#), [D'Orazio et al. \(2016\)](#), [Muñoz & Lai \(2016\)](#), [Miranda et al. \(2017\)](#), [Derdzinski et al. \(2019\)](#), [Muñoz et al. \(2019\)](#), [Mösta et al. \(2019\)](#), [Duffell et al. \(2020\)](#), [Zrake et al. \(2021\)](#), [Muñoz et al. \(2020\)](#), [Muñoz & Lithwick \(2020\)](#), [Derdzinski et al. \(2021\)](#), and Newtonian studies that investigate minidisks include [Farris et al. \(2014\)](#), [Farris et al. \(2015a\)](#), [Tang et al. \(2018\)](#), [Moody et al. \(2019\)](#), [Tiede et al. \(2020\)](#). Studies that use approximate spacetime metrics include [Bowen et al. \(2017\)](#), [Bowen et al. \(2018\)](#), [Bowen et al. \(2019\)](#), [Combi et al. \(2022\)](#). Work that incorporates full GR and MHD include [Farris et al. \(2012\)](#), [Giacomazzo et al. \(2012\)](#), [Gold et al. \(2014a\)](#), [Gold et al. \(2014b\)](#), [Paschalidis et al. \(2021\)](#), [Cattorini et al. \(2021\)](#), and see [Gold \(2019\)](#) for a recent review of work on circumbinary accretion incorporating relativistic effects. Newtonian studies are often conducted as 2D α -disk viscous

hydrodynamics models which have the benefit of being able to evolve for many orbits with less computational expense, but must exclude the inner parts of the domain and impose ad hoc inflow boundary conditions. Such boundary conditions should be informed by relativistic calculations since the inflow time is a parameter in such calculations. General relativity is paramount to treat these inner regions self-consistently.

In our previous work, [Paschalidis et al. \(2021\)](#), we performed the first fully general relativistic simulations of circumbinary accretion onto spinning black holes and investigated the conditions under which persistent minidisks form around the individual black holes. We found that the accretion streams from the circumbinary disk form minidisks whenever there are stable circular orbits around each black hole's Hill sphere. This condition is met when the Hill sphere is significantly larger than the effective innermost stable circular orbit (ISCO). As black hole spin influences the radius of the ISCO, we found that spin plays a crucial role in whether minidisks can form at relativistic orbital separations. We found that at a separation of $d = 20GM/c^2$, black holes with a dimensionless spin parameter of $\chi \equiv cJ/Gm^2 = 0.75$ (where J, m are the black hole angular momentum and mass, respectively) and $\chi = 0$ were able to form minidisks, while black holes with $\chi = -0.75$ were not. The latter is because retrograde spin increases the size of the ISCO significantly, thereby not allowing stable orbits within the Hill sphere at the orbital separations probed by these simulations.

In this work, we extend the simulations presented in our previous work [Paschalidis et al. \(2021\)](#) and present a detailed analysis of the new simulation data. In particular, we examine the structure of the minidisks in greater detail, and investigate the effect that minidisks and black hole spin have on the binary accretion and Poynting outflows, and the quasi-periodic behaviors thereof. One of our most important findings is that *persistent minidisks can dampen the strength of the modulation in the accretion rate*. While we do not investigate in detail the reason why this occurs in this work, our simulations suggest that the inflow time from the minidisks begins to become comparable to the minidisk feeding timescale through the circumbinary accretion streams. This is an important course of study as it can have a significant impact on the observed electromagnetic radiation from black hole binaries, and could affect the interpretation of observed periodicities for systems with much larger minidisks at larger binary orbital separations. This will be the topic of study of future work.

We denote the individual black hole masses as m (all our models contain equal mass binaries $m_1 = m_2 = m$). We adopt geometrized units, $G = c = 1$, throughout the paper.

The rest of the paper is structured as follows: in [Section 2](#) we present our methods, including a description of the models, and numerical methods we adopt in our evolutions. In [Section 3](#) we report our diagnostics used to characterize the accretion flow, EM signatures, minidisk structure, and Fourier analysis. In [Section 4](#) we present the results from analyzing our simulation data. In [Section 5](#) we summarize our findings and discuss future work.

2 METHODS

We employ the following set of assumptions/approximations in each of our models: 1) the black holes are initially on quasi-circular orbits, 2) the self-gravity of the disk is negligible in comparison to the gravity of the binary, 3) the disk is well described by ideal MHD, 4) we do not treat radiative feedback, heating or cooling.

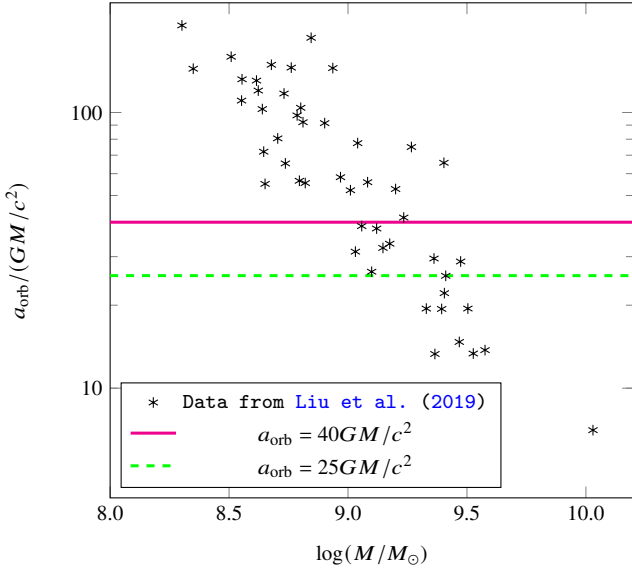


Figure 1. BBH orbital separation (a_{orb} in units of GM/c^2) vs binary total mass M for candidate SMBBHs. Asterisks are data from Liu et al. (2019). The magenta solid (green dashed) line designates an orbital separation of $40GM/c^2$ ($25GM/c^2$). Candidates with $a_{\text{orb}} \lesssim 25GM/c^2$ are in the highly dynamical spacetime regime.

2.1 Initial Data

For a detailed description of the magnetohydrodynamic and spacetime initial data used to start our simulations we refer the reader to Paschalidis et al. (2021). Here we only describe the different black hole configurations which were initially set on quasi-circular orbits at a coordinate separation of $20M$. We consider equal-mass black hole binaries in four spin configurations: $\chi_1 = \chi_2 = 0$ (nonspinning case labeled χ_{00}), $\chi_1 = \chi_2 = 0.75$ (case χ_{++}), $\chi_1 = \chi_2 = -0.75$ (case χ_{--}), $\chi_1 = -\chi_2 = 0.75$ (case χ_{+-}). Where χ_1, χ_2 are the dimensionless spins of each black hole, and $+$ ($-$) sign indicates spin aligned (anti-aligned) with the orbital angular momentum.

2.2 Evolution Equations and Methods

We use the general relativistic magnetohydrodynamics (GRMHD) adaptive-mesh-refinement (AMR), dynamical spacetime code of Etienne et al. (2010), Etienne et al. (2012), which employs the Cactus/Carpet infrastructure Goodale et al. (2003), Schnetter et al. (2004). The code has been extensively tested and used to study numerous systems involving compact objects and magnetic fields.

We evolve the spacetime metric by solving Einstein’s equations in the BSSN formulation Shibata & Nakamura (1995), Baumgarte & Shapiro (1998), coupled to the moving-puncture gauge conditions Baker et al. (2006), Campanelli et al. (2006), with the equation for the shift vector cast in first-order form, as in Hinder et al. (2013). The shift vector parameter η is set to $\eta = 1.375/M$.

We evolve the matter and magnetic fields by solving the ideal GRMHD equations in flux-conservative form (see Eqs. 27-29 in Etienne et al. (2010)) using a high-resolution shock capturing scheme. We enforce the zero-divergence constraint for the magnetic fields by solving the induction equation using a vector-potential formulation (see Eq. 9 in Etienne et al. (2012)). For our EM gauge choice, we use the generalized Lorenz gauge condition developed in Farris

et al. (2012), which avoids the development of spurious magnetic fields across the AMR levels, setting the generalized Lorenz gauge damping parameter to $\xi = 7/M$.

3 DIAGNOSTICS

3.1 MHD Flow Diagnostics

We compute a set of diagnostics to help characterize the MHD flow and the structure and influence of the minidisks. These diagnostics include: 1) The accretion rate \dot{M} as defined in Farris et al. (2010), where we calculate both the total accretion rate onto the binary and the accretion rate onto each individual black hole. 2) The mass within the Hill spheres (i.e. mass of the minidisk in cases where minidisks are present). The Hill Sphere radius is calculated from the Newtonian formula $r_{\text{Hill}} = 0.5(q/3)^{1/3}d$, where q is the mass ratio and d is the binary separation, and we integrate the total rest mass within this radius centered on each black hole. 3) The EM Poynting luminosity L_{EM} on the surface of coordinate spheres S is computed as $L_{EM} = \oint_S T_{0,r}^r dS$, where $T_{\mu,\nu}^{\nu}$ is the EM stress-energy tensor.

3.2 Minidisk Structure Diagnostics

The minidisk structure parameters we calculate are centered on one of the orbiting black holes, but all quantities are computed in the binary center-of-mass frame, as opposed to boosting into the orbiting black hole’s frame. We expect that this would introduce corrections of order $O(v^2) \sim 10\%$, but since the reported diagnostics below are not gauge invariant we do not perform a boost. We use the notation ϖ to indicate the cylindrical radius centered on the orbiting black hole, rather than from the center of the grid.

The minidisk structure parameters we compute are 1) The surface density profile $\Sigma(\varpi)$ of the minidisks, which is computed as defined in Farris et al. (2011) as $\Sigma = \frac{1}{2\pi} \int_0^{2\pi} \int_{z \geq 0} \rho_0 u^t \sqrt{-g} dz d\phi$. 2) The scale height of the minidisks $H(\varpi)/\varpi$, computed as $\Sigma/\rho_0(z=0)$. 3) The effective viscosity parameter $\alpha(\varpi)$ of the minidisks which is calculated as the approximate Shakura-Sunyaev stress parameter and computed as $\alpha = \frac{\langle T_{r\phi}^{EM} \rangle}{\langle P \rangle}$, where $T_{r\phi}^{EM}$ is the orthonormal component of the Maxwell stress-energy tensor evaluated using the tetrad in Penna et al. (2010), and P the pressure. We stress again that none of these diagnostics are gauge-invariant, but moving puncture coordinates are sufficiently well-behaved that the reported quantities provide intuition into the structure of these flows.

3.3 Fourier Analysis

Periodicities are examined by performing Fourier analysis on the time series of several of the output diagnostics. The time series data is treated as follows: first, we subtract the running average by smoothing the data, which is performed using a one-dimensional Gaussian filter, and subtract this smoothed data from the un-smoothed data in order to remove the more general underlying average behavior and isolate the periodic behavior. This smooth-subtracted data is then windowed using the Tukey windowing function. The data is then “zero-padded”, i.e., zeros are added to the end of the data in order to produce a smoother function in frequency space after the Fourier transform is performed without affecting the underlying shape of the function. We then perform a

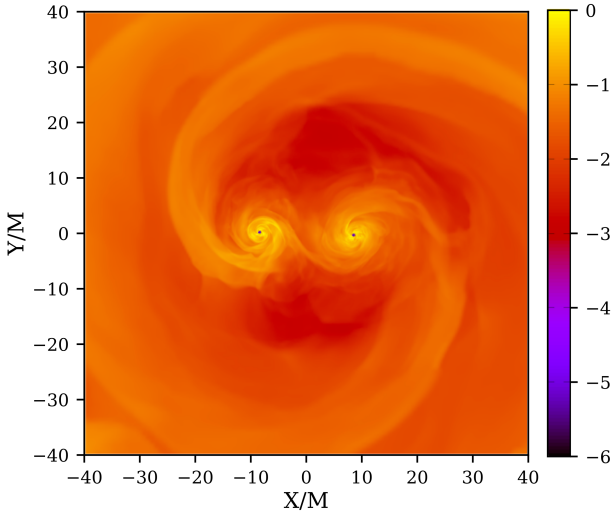


Figure 2. Equatorial rest mass density of the χ_{++} model illustrating the minidisk structures around each black hole after ~ 13 binary orbits.

one-dimensional discrete Fourier transform using the Fast Fourier Transform (FFT) algorithm as implemented in Python using the NumPy Real FFT. The power spectral density (PSD) is then computed as $|FFT|^2$. We normalize the frequencies in the PSD to the orbital frequency of the binary (f_{orb}), which is computed from the average gravitational wave frequency of the $l = 2, m = 2$ mode.

4 RESULTS AND DISCUSSION

4.1 Minidisk Structure

Here we provide a discussion of the structure of the minidisks, which may be used to inform 2D Newtonian simulations that prescribe minidisk quantities, and especially when such structures continue into the relativistic regime.

Fig. 2 shows the rest mass density in the equatorial plane in the χ_{++} model, which exhibits clear persistent minidisks around each of the black holes. Fig. 3 shows the disk parameters $\Sigma(\varpi)$, and $\alpha(\varpi)$ which are the surface density profile of the minidisks, and the effective viscosity of the minidisks, all of which have been azimuthally and time averaged (over ~ 7 full binary orbits) to create a 1D radial profile centered on the minidisk. The parameters reported are calculated for one of the black holes in the χ_{++} model and the positive spin black hole in the χ_{+-} model.

The surface density profile shows the clear presence of a minidisk with a peak surface density around $3.2M$ in the χ_{++} minidisk, and closer to $4M$ in the χ_{+-} minidisk. The effective viscosity parameter α has a value of about 0.02 in most of the χ_{++} disk, and a bit higher in the χ_{+-} disk, and then shoots up to much larger values in the inner region inside of the ISCO as expected. Outside of about $6M$, which is close to the approximate Hill sphere radius at these binary separations, α becomes negative, indicating that the flow in this region is not disk-like, hence it is not a well-defined quantity. Ref. Gold et al. (2014a) also found similar small values of α in the circumbinary disk in cases where they did not use a cooling prescription. The time and azimuthally averaged scale height divided by the radius in the minidisks is approximately constant with $H(\varpi)/\varpi \simeq 0.28$. Thus, minidisks are puffy structures.

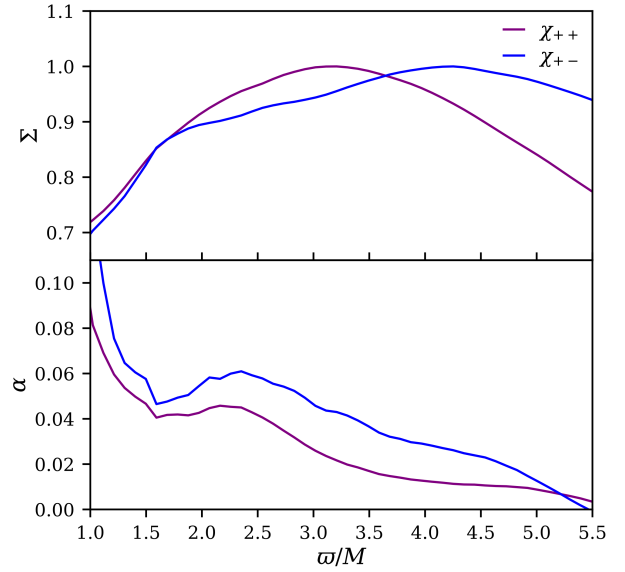


Figure 3. Azimuthally and time averaged minidisk structure parameters for the χ_{++} and χ_{+-} models. *Top:* surface density profile, *bottom:* effective viscosity parameter. Here ϖ indicates the cylindrical radius centered on the black hole. The Hill sphere radius is at about $7M$, and the ISCO radius for the positive spin black hole is $r_{ISCO} = 1.58M$. (Note that here we use $M = m_1 + m_2$ the total mass of the system, not the mass of the individual black hole).

4.2 Variability

In this section we explore the periodic nature of the accretion rates and mass contained within the Hill spheres, as well as the impact of the existence of persistent minidisks on these properties. In this work we build from our previous finding that at our initial separation of $20M$, all black holes in our studies with $\chi = +0.75$ or $\chi = 0$ form persistent minidisks, while all black holes in our studies with $\chi = -0.75$ did not and mass was quickly accreted.

We investigate periodicities through computation of the power spectral density ($PSD = |FFT|^2$) of these signals across each of our models. We normalize the frequencies to the average binary orbital frequency, f_{orb} , for each model.

As noted in our previous work, the time-averaged accretion rate is affected by the black hole spins, with the negatively spinning black holes exhibiting a higher average accretion rate than positively spinning black holes. This is consistent with the negative spin black holes being unable to form minidisks, and thus material from the accretion streams plunges into the BHs directly. Additionally, we found that the average rest-mass within the Hill spheres was much greater for the positively spinning black holes (prograde spin) than the negatively spinning (retrograde spin), again consistent with the formation of persistent minidisks in the positively spinning cases, and hence longer inflow time from the minidisks as opposed to the case where the tidal streams plunge into the black holes. In addition to the difference in time-averaged quantities across our models, we also observe clear periodicities in the accretion rates as well as in the mass within the Hill spheres, which will be the focus of our discussion here.

As shown in the right panels of Fig. 4, we find that all of our models exhibit a definitive peak or peaks in the PSD of the accretion rate, indicating a periodicity at a particular frequency in the accretion. We find the most prominent peak in the PSD

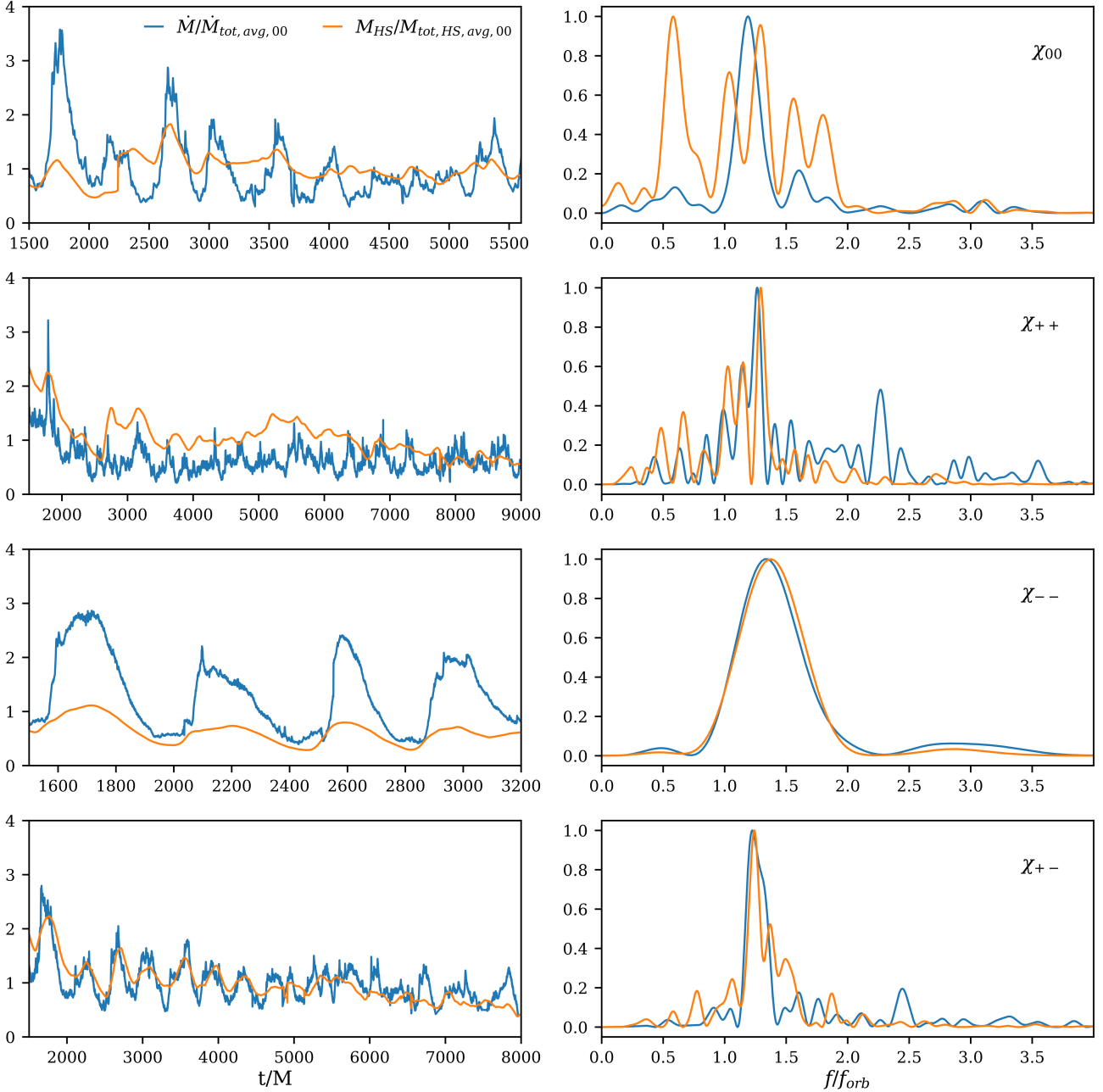


Figure 4. *Left:* Total accretion rate (\dot{M}) (blue curves) and total mass contained within the Hill spheres (M_{HS}) (orange curves) as a function of time for each of our models. From top to bottom we show the χ_{00} , χ_{++} , χ_{--} and χ_{+-} models. We plot the combined total of these quantities for both black holes in all models. Both accretion rate and mass within the Hill spheres exhibit periodic fluctuations with time that are mostly in phase with one another. The reported quantities are normalized by their respective average values in the χ_{00} model to provide a consistent normalization across all models. *Right:* PSD of the accretion rate and mass within the Hill spheres shown in the corresponding left panel normalized to the peak value of the PSD in each case.

of the accretion rate in all models falls between $\sim 1.2 - 1.4 f_{orb}$ consistent with previous studies Noble et al. (2012); Shi & Krolik (2015); Bowen et al. (2018, 2019); Combi et al. (2022). The PSD of the mass contained within the Hill spheres shows strong peaks that closely match those in the accretion rates in each model. The χ_{00} case also exhibits several other strong peaks in the PSD of the mass contained within the Hill spheres that are not present in the accretion rate, the strongest of which occur at $\sim f_{orb}$ and $\sim 0.5 f_{orb}$.

We also find that the modulations in the accretion rates and the

mass within the Hill spheres are predominantly in phase, as shown in the left panels of Fig. 4. This correlation between the frequencies and phase of the modulations in the accretion and the mass within the Hill spheres is not surprising, as cycles of increased rest-mass within the Hill spheres leads directly to an increase in the rest-mass accreted onto the black holes. This is in agreement with the findings of Combi et al. (2022), which describes the time-dependence of the minidisk mass as a smoothed version of that of the accretion rates.

We further investigate the relative strength of the modulation

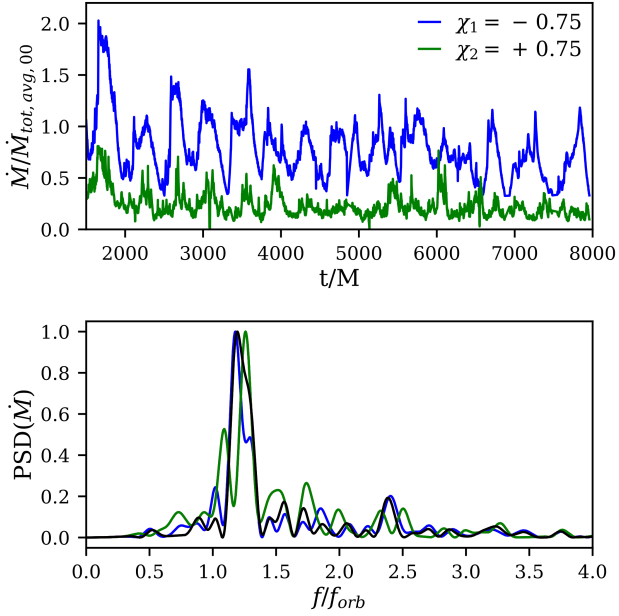


Figure 5. *Top:* Accretion rates onto the individual black holes in the χ_{+-} model, illustrating the effect of the minidisk around the positively spinning black hole causing a significantly dampened amplitude in the modulation of the accretion rate compared to the negatively spinning black hole where no minidisk is present. *Bottom:* PSD of the above accretion rates, with the black curve representing the PSD of the total accretion rate. Each PSD is normalized to its own peak value.

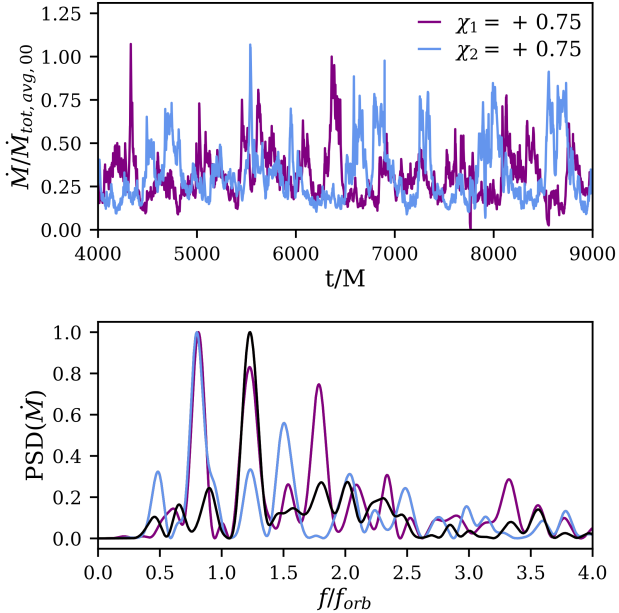


Figure 6. *Top:* Accretion rates onto the individual black holes in the χ_{++} model. *Bottom:* PSD of the above accretion rates, with the black curve representing the PSD of the total accretion rate. Each PSD is normalized to its own peak value.

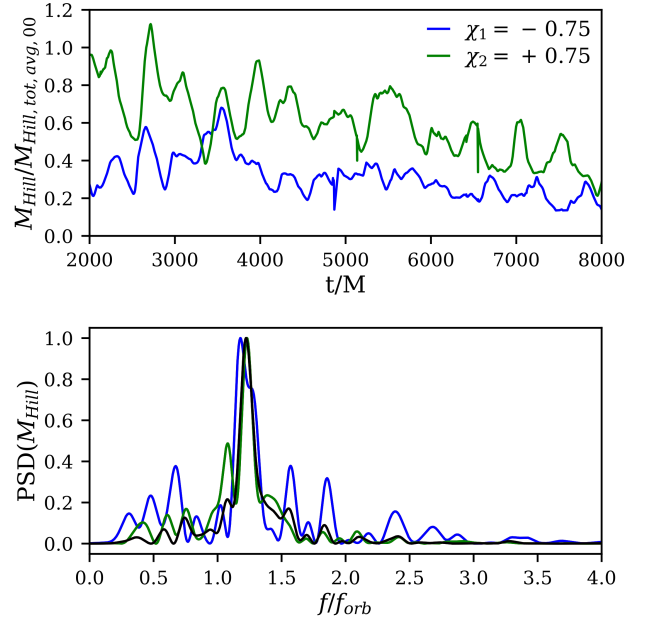


Figure 7. *Top:* Masses within the Hill spheres of the individual black holes in the χ_{+-} model. *Bottom:* PSD of the above masses, with the black curve representing the PSD of the total mass contained in both Hill spheres. Each PSD is normalized to its own peak value.

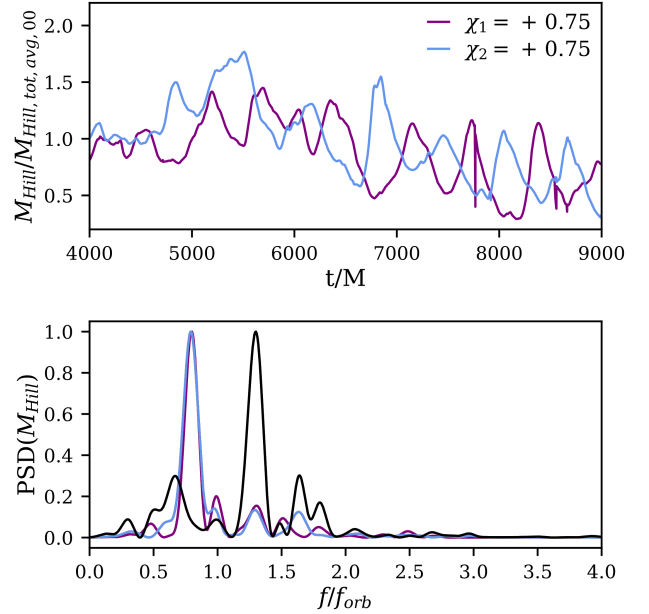


Figure 8. *Top:* Masses within the Hill spheres of the individual black holes in the χ_{++} model. *Bottom:* PSD of the above masses, with the black curve representing the PSD of the total mass contained in both Hill spheres. Each PSD is normalized to its own peak value.

by comparing the amplitudes of the variability in the accretion rates and mass within the Hill spheres. This demonstrates that the modulation is strongest in the negative spinning model, and becomes weaker with increasingly positive spin. This can be seen easily in the amplitudes of the variability in the left panel of Fig. 4 by contrasting the χ_{00} , χ_{++} , and χ_{--} models (top three panels). This is also clearly demonstrated by comparing the accretion rates onto the individual black holes in the χ_{+-} case as seen in Fig. 5. These demonstrate that *the presence of a persistent minidisk not only slows the accretion rate, but also suppresses the strength of the quasi-periodic modulation in the accretion rate.*

We quantify this by calculating the ‘‘average deviation’’, which measures the average distance of the data set from the mean accretion rate, as well as calculating the root-mean-square (RMS). These values are reported in Table 1. Note that since the accretion rates are normalized by the average accretion rate in the χ_{00} , this allows us to compare the amplitudes of the variation in each model. Also note that these normalized accretion rates are of order unity (see left panels of Fig 4), hence the numbers reported in Table 1 can be viewed as crude percentage-level fluctuations. We find a monotonic decrease in both the average deviation and the RMS with increasing spin values in the χ_{--} , χ_{00} , and χ_{++} models, with a factor of ~ 3 decrease in both the RMS and the average deviation comparing the χ_{++} model to the χ_{--} model. In last two rows of the table we also report the RMS and average deviation from the mean in the χ_{+-} case for each black hole separately, where it is clear that the prograde spin black hole exhibits much smaller fluctuations than the retrograde spin black hole.

These results demonstrate that the existence of persistent minidisks is strongly correlated with a decreased strength of the variability in the accretion rate onto the black holes. Given that higher spins, thus existence of persistent minidisks, are also associated with lower accretion rates (seen clearly in Fig. 5), these results suggest that for larger minidisks, the dampening of the fluctuations arises because the inflow time from the minidisks begins to become comparable to the minidisk feeding timescale through the circumbinary accretion streams.

The above conclusion may impact the interpretation of observed periodicities in quasars as arising by the modulation of the accretion rate onto the binary. Binaries at larger separations and therefore larger Hill spheres and potentially much larger minidisks may have periodicities dampened even more, and it is unclear whether they will be able to exhibit any observable periodicities. Therefore, quasi-periodic behavior in observed lightcurves arising from modulations in the accretion rate may not be smoking-gun evidence for the existence of a binary. More work is necessary to shed light on this important effect, which will be the subject of a future paper.

We further examine the nature of the periodic behavior by analyzing the accretion rates and masses within the Hill spheres for the individual black holes for the χ_{+-} and χ_{++} models. These can be found in Figs. 5, 6, 7, 8, along with the PSDs of these quantities.

We find that the individual accretion rates onto the two black holes in the χ_{+-} model appear to have the modulation of their accretion rates to be mostly in phase, and the PSD of the individual and total accretion rates all exhibit the same peak frequency, which can be seen in Fig. 5. A very similar pattern is seen in the mass within the Hill spheres of the individual black holes in the χ_{+-} model, where the variability is roughly in phase, and the PSD exhibits the same peak frequency for each black hole as well as the total mass contained in both Hill spheres, which can be seen in Fig. 7. Conversely, the individual accretion rates in the χ_{++} model

Table 1. Root-mean square (RMS) and average deviation of the accretion rates in each of our models. All values are normalized by the same value of the average accretion rate in the χ_{00} model. Note that the values reported for the χ_{++} , χ_{00} , and χ_{--} are for the total accretion rate onto both black holes, while the values of the χ_{+-} model are reported for the accretion rates onto the individual black holes.

Model	RMS	Average Deviation
χ_{++}	0.21	0.17
χ_{00}	0.49	0.38
χ_{--}	0.65	0.57
$\chi_{+-,+}$	0.10	0.078
$\chi_{+,-}$	0.28	0.22

appear mostly out of phase. The PSD of the individual accretion rates exhibit peak frequencies at $\sim 0.75f_{orb}$, close to half of the peak frequency of the total accretion rate (at which the individual accretion rates also exhibit peaks in the PSD albeit with reduced power), which can be seen in Fig. 6. The same trend is present in the mass within the individual Hill spheres in the χ_{++} model, with the modulation out of phase, and the strongest peak in the individual PSDs at $\sim 0.75f_{orb}$, and the strongest peak in the total Hill spheres mass PSD at $\sim 1.2f_{orb}$, which can be seen in Fig. 8.

4.3 Outflows and Jets

We observe collimated, highly magnetized outflows from the polar regions of the black holes. In Fig. 9 we show meridional slices of the magnetic-to-rest-mass energy density $b^2/2\rho_0$ of the χ_{++} , χ_{+-} , and χ_{00} models. The large values of $b^2/2\rho_0$ found in the outflows indicate that these regions are magnetically dominated and the jets are magnetically powered. These regions are nearly force-free, which is a requirement for the Blandford-Znajek (BZ) mechanism Blandford & Znajek (1977). We find significantly higher values of $b^2/2\rho_0$ in our spinning cases than previous non-spinning fully relativistic binary accretion studies (see e.g. Gold et al. (2013); Gold et al. (2014b)). The χ_{++} model shows both black holes generating strongly magnetized outflow regions, while in the χ_{+-} model, the positive spin black hole has a magnetized outflow region which dominates over that of the negative spin black hole. This is in agreement with Tchekhovskoy & McKinney (2012), which found that single black holes with spins prograde with the accretion disk have more powerful jets than black holes with retrograde spins. The χ_{00} model shows significantly less strongly magnetized outflows, indicating that the spin of the black holes plays the predominant role in the magnetization strength. The significantly enhanced magnetization and outgoing Poynting luminosity in the χ_{++} and χ_{+-} models compared to the χ_{00} model, demonstrates that the traditional spin-induced BZ effect dominates over the ‘‘orbital’’ BZ effect Palenzuela et al. (2010). This also demonstrates that the boost in Poynting luminosities reported post-merger in simulations of initially non-spinning black holes Gold et al. (2014a,b); Khan et al. (2018) is due to the fact that accretion onto the remnant black hole proceeds onto a spinning black hole.

We also examine the Poynting luminosities (calculated far away from the binary-disk system and considered only after the quantity settles following the initial burst) and their PSDs focusing on the χ_{+-} and χ_{++} cases, which can be seen in Fig. 10. Both the χ_{+-} and χ_{++} models show a clear peak in the PSD of the Poynting luminosity, though they do not have their peaks at the same frequency across the models like was seen in the accretion rates. In the PSD of the

8 Bright & Paschalidis

χ_{+-} model, we see a peak at $\sim 1.2f_{orb}$, approximately equal to the peak seen in the PSD of the accretion rate (either total or onto the individual black holes). However, the PSD of the χ_{++} model has its peak at $\sim 0.6f_{orb}$, about half of the peak seen in the PSD of the total accretion rate. However, this is approximately equal to the dominant peaks seen in the individual accretion rates. It is unclear as to why this is the case, but in our case we compute the luminosities on the surface of a distant sphere that encompasses the entire binary+circumbinary disk system. In the χ_{+-} case the Poynting luminosity is dominated by the prograde spin BH hence the prograde spin accretion rate variability is reflected in the jet. Given that the accretion time series onto the individual black holes in the χ_{++} are not in phase, it is not unreasonable to expect that the Poynting luminosity exhibits a periodicity at the accretion rate periodicity onto the individual BHs, which exhibit peak observed variability at $\sim 1/2$ of the main frequency of the total accretion rate.

5 CONCLUSIONS

We have continued our work from Paschalidis et al. (2021) to extend the evolution of our GRMHD simulations in full GR and further our analysis of minidisks and black hole spin in accreting SMBH binaries.

We present details of the structure of minidisks through 1D orbit and time averaged profiles of the surface density, scale height, and effective viscosity that may be helpful to inform the parameters used in Newtonian studies in which binaries approach the relativistic regime.

We examine the periodic behaviors of the mass of the minidisks, the accretion rates, and the Poynting luminosities, and make comparisons across our four models. We find a clear peak in the PSD of both the total mass of the minidisks and total accretion rates corresponding to $\sim 1.2 - 1.4f_{orb}$, which is consistent with previous simulations. We find this peak to be present in all of our models, regardless of spin or presence of minidisks. We find a peak at roughly the same frequency in the Poynting luminosity of the χ_{+-} model, and at roughly half that frequency in the χ_{++} model, which is correlated with the modulation frequency of the accretion rates onto the individual black holes in the system.

While the peak frequency of the periodicity is consistent across our models, the strength of the modulation is not. We find a factor of ~ 3 reduction of the average deviation and the RMS variability in the accretion rates in positively spinning black holes that exhibit minidisks compared to the negatively spinning black holes where no minidisks are present. This is found both in comparing the accretion rates of the χ_{++} and χ_{--} models, and the individual black holes in the χ_{+-} model. This indicates that the presence of minidisks works to dampen out the strength of the periodic nature of the accretion onto the black holes. At larger separations, and thus larger Hill spheres and larger minidisks, it is possible that the variability may be dampened out even further, leading to little or no periodicities at larger separations. In future work we will investigate simulations at larger separations to better probe the behavior of larger minidisks and periodic behaviors.

ACKNOWLEDGEMENTS

This work was in part supported by NSF grants PHY-1912619 and PHY-2145421 to the University of Arizona, as well as NSF Graduate Research Fellowship grant DGE-1746060. Computational resources

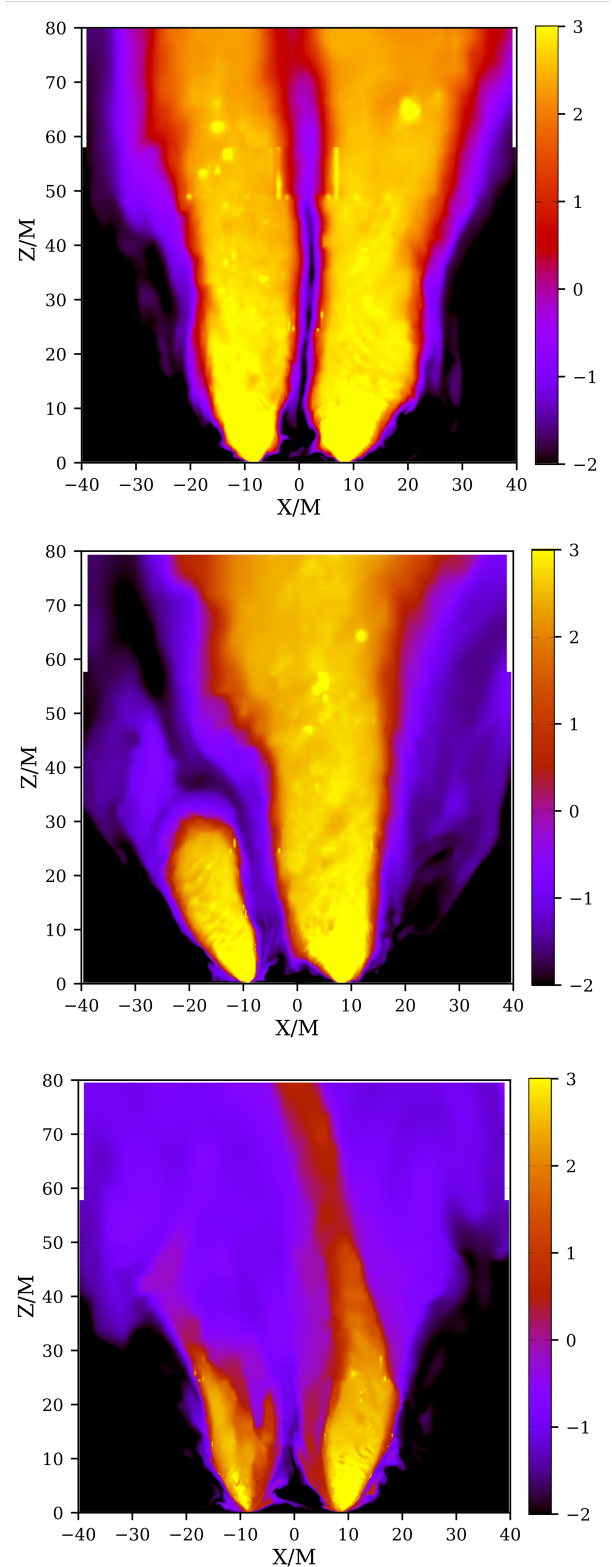


Figure 9. Meridional slice of magnetization $\log(b^2/2\rho_0)$ for the χ_{++} (top panel), χ_{+-} (middle panel), χ_{00} (bottom panel). The snapshot is chosen at a time where both black holes are located along the X-axis in their orbits, with the positive spin black hole on the right (positive X-position) and the negative spin black hole on the left (negative X-position) for the χ_{+-} case. The snapshots are taken after 13, 10, and 12 binary orbits respectively for the χ_{++} , χ_{+-} , and χ_{00} models.

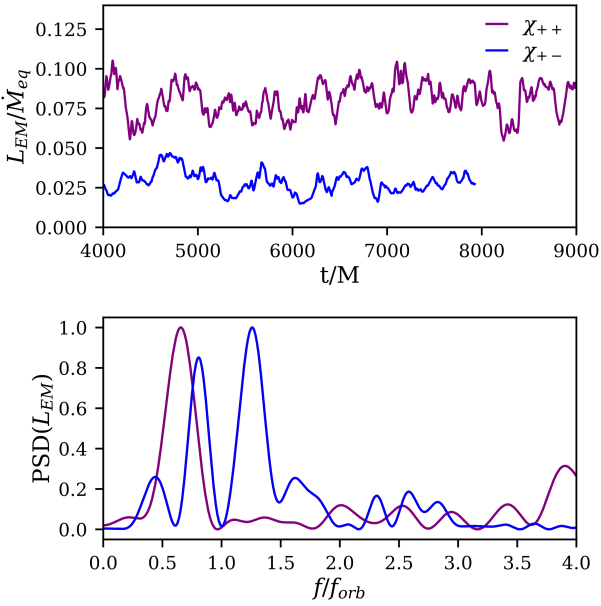


Figure 10. *Top:* Poynting luminosity, L_{EM} , as a function of time for the χ_{++} and χ_{+-} models. *Bottom:* PSD of the Poynting luminosities for each model normalized to the peak value of the PSD in each case.

were provided by the Extreme Science and Engineering Discovery Environment (XSEDE) under grant No. TG-PHY190020. XSEDE is supported by the NSF grant No. ACI-1548562. Simulations were performed on Comet, and Stampede2, which is funded by the NSF through award ACI-1540931.

DATA AVAILABILITY

The data underlying this article will be shared on reasonable request to the corresponding author.

REFERENCES

- Amaro-Seoane P., et al., 2017, arXiv e-prints, p. arXiv:1702.00786
 Amaro-Seoane P., et al., 2022, arXiv e-prints, p. arXiv:2203.06016
 Artymowicz P., Lubow S. H., 1994, *ApJ*, **421**, 651
 Arun K. G., et al., 2022, *Living Reviews in Relativity*, **25**, 4
 Baker J. G., Centrella J., Choi D.-I., Koppitz M., van Meter J., 2006, *Phys. Rev. Lett.*, **96**, 111102
 Barausse E., et al., 2020, *General Relativity and Gravitation*, **52**, 81
 Baumgarte T. W., Shapiro S. L., 1998, *Phys. Rev. D*, **59**, 024007
 Blandford R. D., Znajek R. L., 1977, *MNRAS*, **179**, 433
 Bogdanović T., Miller M. C., Blecha L., 2022, *Living Reviews in Relativity*, **25**, 3
 Bowen D. B., Campanelli M., Krolik J. H., Mewes V., Noble S. C., 2017, *ApJ*, **838**, 42
 Bowen D. B., Mewes V., Campanelli M., Noble S. C., Krolik J. H., Zilhão M., 2018, *ApJ*, **853**, L17
 Bowen D. B., Mewes V., Campanelli M., Noble S. C., Avara M., Campanelli M., Krolik J. H., 2019, *ApJ*, **879**, 76
 Campanelli M., Lousto C. O., Marronetti P., Zlochower Y., 2006, *Phys. Rev. Lett.*, **96**, 111101
 Cattorini F., Giacomazzo B., Haardt F., Colpi M., 2021, *Phys. Rev. D*, **103**, 103022
 Charisi M., Bartos I., Haiman Z., Price-Whelan A. M., Graham M. J., Bellm E. C., Laher R. R., Márka S., 2016, *MNRAS*, **463**, 2145

- Combi L., Lopez Armengol F. G., Campanelli M., Noble S. C., Avara M., Krolik J. H., Bowen D., 2022, *ApJ*, **928**, 187
 D’Orazio D. J., Di Stefano R., 2018, *MNRAS*, **474**, 2975
 D’Orazio D. J., Haiman Z., MacFadyen A., 2013, *MNRAS*, **436**, 2997
 D’Orazio D. J., Haiman Z., Schiminovich D., 2015, *Nature*, **525**, 351
 D’Orazio D. J., Haiman Z., Duffell P., MacFadyen A., Farris B., 2016, *MNRAS*, **459**, 2379
 Derdzinski A. M., D’Orazio D., Duffell P., Haiman Z., MacFadyen A., 2019, *MNRAS*, **486**, 2754
 Derdzinski A., D’Orazio D., Duffell P., Haiman Z., MacFadyen A., 2021, *MNRAS*, **501**, 3540
 Duffell P. C., D’Orazio D., Derdzinski A., Haiman Z., MacFadyen A., Rosen A. L., Zrake J., 2020, *ApJ*, **901**, 25
 Etienne Z. B., Liu Y. T., Shapiro S. L., 2010, *Phys. Rev. D*, **82**, 084031
 Etienne Z. B., Paschalidis V., Shapiro S. L., 2012, *Phys. Rev. D*, **86**, 084026
 Farris B. D., Liu Y. T., Shapiro S. L., 2010, *Phys. Rev. D*, **81**, 084008
 Farris B. D., Liu Y. T., Shapiro S. L., 2011, *Phys. Rev. D*, **84**, 024024
 Farris B. D., Gold R., Paschalidis V., Etienne Z. B., Shapiro S. L., 2012, *Phys. Rev. Lett.*, **109**, 221102
 Farris B. D., Duffell P., MacFadyen A. I., Haiman Z., 2014, *ApJ*, **783**, 134
 Farris B. D., Duffell P., MacFadyen A. I., Haiman Z., 2015a, *MNRAS*, **446**, L36
 Farris B. D., Duffell P., MacFadyen A. I., Haiman Z., 2015b, *MNRAS*, **447**, L80
 Giacomazzo B., Baker J. G., Miller M. C., Reynolds C. S., van Meter J. R., 2012, *ApJ*, **752**, L15
 Gold 2019, *Galaxies*, **7**, 63
 Gold R., Paschalidis V., Etienne Z. B., Shapiro S. L., Pfeiffer H. P., 2013
 Gold R., Paschalidis V., Etienne Z. B., Shapiro S. L., Pfeiffer H. P., 2014a, *Phys. Rev. D*, **89**, 064060
 Gold R., Paschalidis V., Ruiz M., Shapiro S. L., Etienne Z. B., Pfeiffer H. P., 2014b, *Phys. Rev. D*, **90**, 104030
 Goodale T., Allen G., Lanfermann G., Massó J., Radke T., Seidel E., Shalf J., 2003, in *Vector and Parallel Processing – VECPAR’2002*, 5th International Conference, Lecture Notes in Computer Science. Springer, Berlin, <http://edoc.mpg.de/3341>
 Graham M. J., et al., 2015, *MNRAS*, **453**, 1562
 Hinder I., et al., 2013, *Classical and Quantum Gravity*, **31**, 025012
 Hobbs G., et al., 2010, *Classical and Quantum Gravity*, **27**, 084013
 Khan A., Paschalidis V., Ruiz M., Shapiro S. L., 2018, *Phys. Rev. D*, **97**, 044036
 Kocsis B., Haiman Z., Loeb A., 2012, *MNRAS*, **427**, 2660
 Liu T., et al., 2019, [10.3847/1538-4357/ab40cb](https://arxiv.org/abs/10.3847/1538-4357/ab40cb)
 MacFadyen A. I., Milosavljević M., 2008, *ApJ*, **672**, 83
 Mayer L., Kazantzidis S., Madau P., Colpi M., Quinn T., Wadsley J., 2007, *Science*, **316**, 1874
 Milosavljević M., Phinney E. S., 2005, *ApJ*, **622**, L93
 Miranda R., Muñoz D. J., Lai D., 2017, *MNRAS*, **466**, 1170
 Moody M. S. L., Shi J.-M., Stone J. M., 2019, *ApJ*, **875**, 66
 Mösta P., Taam R. E., Duffell P. C., 2019, *ApJ*, **875**, L21
 Muñoz D. J., Lai D., 2016, *ApJ*, **827**, 43
 Muñoz D. J., Lithwick Y., 2020, *ApJ*, **905**, 106
 Muñoz D. J., Miranda R., Lai D., 2019, *ApJ*, **871**, 84
 Muñoz D. J., Lai D., Kratter K., Miranda R., 2020, *ApJ*, **889**, 114
 Noble S. C., Mundim B. C., Nakano H., Krolik J. H., Campanelli M., et al., 2012, *Astrophys. J.*, **755**, 51
 Noble S. C., Krolik J. H., Campanelli M., Zlochower Y., Mundim B. C., Nakano H., Zilhão M., 2021, *ApJ*, **922**, 175
 Palenzuela C., Garrett T., Lehner L., Liebling S. L., 2010, *Phys. Rev. D*, **82**, 044045
 Paschalidis V., Bright J., Ruiz M., Gold R., 2021, *ApJ*, **910**, L26
 Penna R. F., McKinney J. C., Narayan R., Tchekhovskoy A., Shafee R., McClintock J. E., 2010, *MNRAS*, **408**, 752
 Rodriguez C., Taylor G. B., Zavala R. T., Pihlström Y. M., Peck A. B., 2009, *ApJ*, **697**, 37
 Roedig C., Krolik J. H., Miller M. C., 2014, *ApJ*, **785**, 115
 Schnetter E., Hawley S. H., Hawke I., 2004, *Classical and Quantum Gravity*, **21**, 1465

- Sesana A., Roedig C., Reynolds M. T., Dotti M., 2012, [MNRAS](#), **420**, 860
- Shi J.-M., Krolik J. H., 2015, [ApJ](#), **807**, 131
- Shi J.-M., Krolik J. H., Lubow S. H., Hawley J. F., 2012, [ApJ](#), **749**, 118
- Shibata M., Nakamura T., 1995, [Phys. Rev. D](#), **52**, 5428
- Tang Y., Haiman Z., MacFadyen A., 2018, [MNRAS](#), **476**, 2249
- Tehekhoyskoy A., McKinney J. C., 2012, [MNRAS](#), **423**, L55
- Tiede C., Zrake J., MacFadyen A., Haiman Z., 2020, [ApJ](#), **900**, 43
- Zrake J., Tiede C., MacFadyen A., Haiman Z., 2021, [ApJ](#), **909**, L13

This paper has been typeset from a \TeX/L\TeX file prepared by the author.